Quad-band Multiple Input Multiple Output Modified PIFA Antenna for WLAN and LTE Mobile Applications

Reza Khajeh Mohammad Lou [1, 2*], Tohid Aribi [1,2], Tohid Sedghi[3, 4]
1- Department of Electrical Engineering, Miandoab Branch, Islamic Azad University, Miandoab, Iran.
Email: reza.mohammadlou63@gmail.com (Corresponding author)
2- Artificial Intelligence and Big Data Automation Research Center, Urmia Branch, Islamic Azad University, Urmia, Iran.
Email: tohidaribi@gmail.com
3- Department of Electrical Engineering, Urmia Branch, Islamic Azad University, Urmia, Iran.
4- Microwave and Antenna Research Center, Urmia Branch, Islamic Azad University, Urmia, Iran.
Email: sedghi.tohid@gmail.com

Received: 2 January 2023 Revised: 10 February 2023 Accepted: 15 March 2023

ABSTRACT:
In this article, a multiple input multiple output quadrate frequency bands modified PIFA antenna is introduced for 4G LTE and WLAN applications. The quadrate proposed antenna covers LTE 1800 (1.71-1.88 GHz), LTE 1900 (1.85-1.99 GHz), UMTS (1.92-2.17 GHz), LTE 2300 (2.305-2.400 GHz), LTE 2500(2.50-2.69 GHz), WLAN (2.400-2.484 GHz-5.15-5.75 GHz) specified by IEEE 802.11a/b/g/n/ac and WiMAX (3.3–3.6 GHz). Then, the PIFA antenna is used as 2×1 MIMO antenna as a radiation element. The overall dimensions of the single antenna are 50×35×0.8 mm^3 and the MIMO antenna is 50×70×0.8 mm^3 while both are realized on FR4-epoxy substrate. To reduce mutual coupling between PIFA antennas at MIMO configuration, Defected Ground Structure (DGS) along with parasitic double split ring resonator is used. The antenna performance is confirmed by the construction of the antenna prototype and measuring its characteristics in terms of reflection loss coefficient, gain, and radiation properties. The extracted outcomes show a good correlation between the simulation and experimental results that candidate it to satisfy mobile communication requirements.

KEYWORDS: LTE, MIMO, Multi-Band, PIFA, EBG.

1. INTRODUCTION

Because of rapid development of technology and the explosion of people's demands on high data rate wireless communication, nowadays mobile devices need to operate in multiband functionality along with support various communication standards [1], [2]. Hence appropriate design is required so that a single compact antenna operates simultaneously in ISM and 4G LTE bands [3]. Furthermore, such antenna should satisfy the requirements of communication systems such as low profile, ease fabrication process and miniaturized size to fit it in the mobile equipment [4].

Recently, several antenna design processes have been studied to obtain multiband operation at 4G and WLAN frequency bands. Various designs and techniques of microstrip antennas have been noticed in the literature to utilize in multiband applications such as conventional planar inverted F antenna, fractal geometry, multiple current path technique, and multi resonance metamaterial patches [4-7]. However, these multiband design techniques have some drawbacks that cause the antenna features could not be easily accustomed. The problems with these include design complexity, vulnerable to the outside interface, size, mutual coupling between resonators, and high cost [8, 9]. Also, in order to achieve high capacity and overcome the multipath fading phenomenon, multiple output multiple input (MIMO) technique has been extensively used in wireless communication systems [10-13]. Various printed MIMO antenna systems have been proposed over the years that work at 4G and WLAN frequencies [14-17]. However, such a method causes to more challenges to the antenna design including MIMO antenna size and mutual coupling between radiation elements in MIMO configuration which directly affects the antenna performance. Therefore, the main objective is to keep a compact size and good isolation. To achieve these goals, several methods have been studied by many researchers, including spatial separation and back-to-back configuration between antennas, defected ground

Paper type: Research paper
DOI: 10.30486/mjee.2023.1976700.1047.
How to cite this paper: R. Khajeh Mohammad Lou, T. Aribi and T. Sedghi, **"Quad-band Multiple Input Multiple Output Modified PIFA Antenna for WLAN and LTE Mobile Applications"**, *Majlesi Journal of Electrical Engineering*, Vol. 17, No. 2, pp. 99-108, 2023.

structure concept and electromagnetic bandgap structure [18-23]. A design of printed 2×2 MIMO antennas presented in [3] is composed of two inverted F-shaped monopoles that support dual bands operation from 2.25 to 3.32 GHz, and from 3.32 to 3.74 GHz covering long LTE 2300/2500 bands, WLAN 2.4 GHz and WIMAX. The proposed antennas are showing poor isolation at upper-frequency bands.

Another design of MIMO antennas was proposed by developing two PIFAs in [11] for LTE 2500 (2.57-2.64 GHz) and WLAN 5 GHz upper UNII band (5.725-5.825 GHz). However, the antenna is well matched at all desired frequencies with values below -15 dB, and the size of the antenna is 40×75×1.6 mm^3, which cannot be suitable for compact mobile devices.

Another design of multiband MIMO antennas based on coupled fed monopole in a meandered shape is presented in [12]. It is capable of covering LTE 1800/1900/2500, UMTS, and WLAN 2.4GHz frequency bands.

The isolation between radiation elements is achieved by dual decoupling structures consisting of ground slots and inverted L ground branches. The isolation is obtained better than 15 dB over all the frequency bands. However, the overall dimension of the antenna is 110 × 65 × 0.8 mm^3 which is highly inappropriate for modern-day smartphones.

The current study presents a modified design of PIFA antenna for multiband operation. Multiband functionality is accomplished by a blend of creating additional effective current paths to the conventional PIFA antenna in the limited space and square complementary split ring resonator (SCSRR) along with dual asymmetrical stubs on the antenna's ground-plane. The modified PIFA antenna covers simultaneously the following operational bands: LTE 1800 (1.71-1.88 GHz), LTE 1900 (1.85-1.99 GHz), UMTS (1.92-2.17 GHz), LTE 2300 (2.305-2.400 GHz), LTE 2500(2.50-2.69 GHz), WLAN (2.4-2.484 GHz and 5.15-5.75 GHz) specified by IEEE 802.11a/b/g/n/ac and WiMAX (3.3–3.6 GHz). The resonance band centered at LTE, UMTS, and 2.4GHz wireless ISM bands are associated with a quarter guided-wavelength effective current path meanwhile the resonance band is attributed to 5GHz WLAN specification which is achieved by the SCSRR unit cell with stubs on the ground. Then the modified PIFA antenna has been used as a radiation element in 2×2 MIMO configuration. A combination of novel procedures has been used to diminish the mutual coupling between two elements. These methods used include: (1) Positioning the antenna opposite to each other in order to eliminate opposite fields; (2) Utilizing the defective ground structure; (3) Embedding the double split ring resonator as electromagnetic bandgap structure between elements. The proposed methods are confirmed through simulation, construction, and measurement. Details of the antenna design parameters are investigated numerically and experimentally. The outcomes show appropriate agreement between experimental and simulation results that make it the right choice for wireless communication. The article is ordered in this manner: Section II describes the suggested modified PIFA antenna configuration along with its parametric studies; Section III presents the 2×2 MIMO configurations and simulation results; Section IV reports the measurement results of the fabricated antenna; and lastly, Section V summarizes the study.

2. DESIGN OF MODIFIED PIFA ELEMENT

2.1. Antenna Configuration

The geometry and physical parameters of the final proposed modified PIFA antenna and systematic step-by-step configuration are shown in Fig. 1. It comprises a patch including a resembling inverted-F radiation element and a metamaterial unit-cell that is located on FR4 dielectric substrate with permittivity of 4.4 and thickness of 0.8 mm. The dimension of the substrate is 50×38 mm^2 and the 50 Ω microstrip line is used to feed the patch. Also, Fig. 1(b) shows five steps to realize the proposed PIFA antennas, namely:

Step I) Create a conventional inverted F as a radiating patch (Ant. I).

Step II) Add a stub to the ground plane to optimize impedance matching and bandwidths antenna (Ant. II)

Step III) Add strip line as the current path to Ant. II to create dual band functionality that resonates at LTE 1800& 2100 and WiMAX (Ant. III).

Step IV) Add another strip line opposed to the previous step that leads to the production of the LTE 2500 and 2.4 GHz WLAN bands (Ant. IV).

Step V) Add a square complementary split ring resonator (SCSRR) near the feed line on the substrate along with a stub on the ground plane to cover 5 GHz WLAN bands.

The proposed PIFA antenna geometry was adjusted by parametric analyses using High-Frequency simulation software (HFSS ver. 15) and the optimal dimension of the designed antenna is shown in Table 1.

Table 1. Dimension of the element in mm.

L=50	W=35	L_f=30	W_f=1.5	g_s=1	L_s=12	L_{gm}=2.25
L_{sm}=4.5	**L_g=8**	**g=1**	**L_F=14**	**W_1=2.5**	**L_{s1}=19.75**	**L_{s2}=12.75**
L_{s3}=15	**L_{s4}=5**	**L_{s5}=4**	**L_{s6}=3**	**L_{m1}=3**	**L_{m2}=2**	**L_m=4.5**
g_m=0.25	**g_p=0.5**	**g_1=1**	**L_{si}=6**	**L_{so}=8**	**L_{si1}=4.5**	**L_{so1}=6**
L_{f1}=8	**W_{f1}=7**	**W_{g1}=6**	**L_{f2}=16**	**L_{f3}=4**	**W_{g2}=2**	**W_m=70**

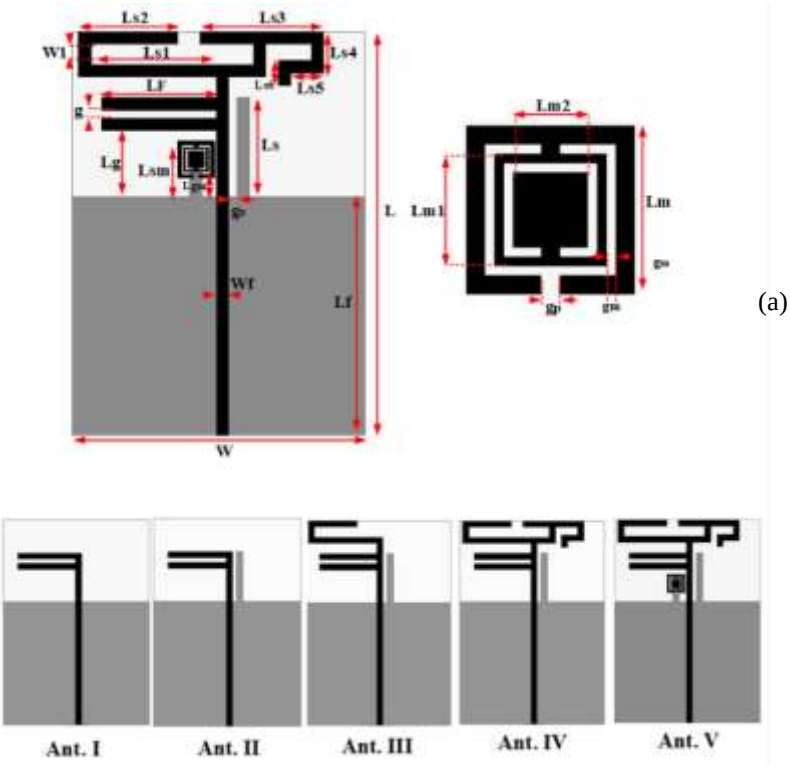

Fig. 1. (a) configuration of the antenna (b) Steps taken in the progress of the suggested PIFA antenna.

Fig. 2 shows the plot of the S-parameters of the SCRR structure, which is obtained from the analysis of a unit-cell due to the homogeneity of the structure, which is desired. As it is obvious, the resonant frequency of this structure is in the WLAN. This geometry leads to the improvement of the upper-band performance.

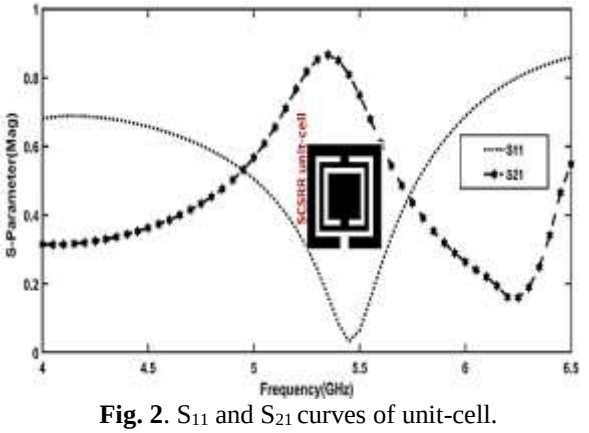

Fig. 2. S_{11} and S_{21} curves of unit-cell.

2.2. Parametric Study of Antenna

In this section, the PIFA antenna is modeled numerically and simulated using the HFSS simulator software. The effect of individual parameters on the act of antenna evolution, presented in the previous section, was studied in terms of return loss coefficient, and radiation patterns. The dimension of the final PIFA antenna was determined through the optimization process by varying the parameter in question while keeping all other parameters fixed. The S_{11} response of Ant. I up to Ant. V are simulated and depicted based on Important parameters influencing performance of each antenna. First, the resonance frequency of the conventional PIFA antenna (Ant. I) has been investigated for different lengths of the gap between the ground plane and F shape patch (L_g) along with the effect of varying the dimension of F- shaped stubs length (L_F). Fig. 3 shows the consequence of L_g and L_F on the S_{11} response of Ant. I. It was observed that for Ant. I, these parameters have a main effect on the antenna's impedance matching at lower and upper-frequency bands. As it is clear from the figure, the patch's lower resonance frequency is very sensitive to the distance between the ground plane and inverted F patches while the variation of L_F has the greatest impact on the higher band. The operating frequency bands corresponding to Ant. I are confined between 2.25-2.94 GHz and 3.24- 3.3 GHz with a $S_{11} \leq$ -10 dB at the optimum value of L_g= 38 mm and L_F=15.5 mm.

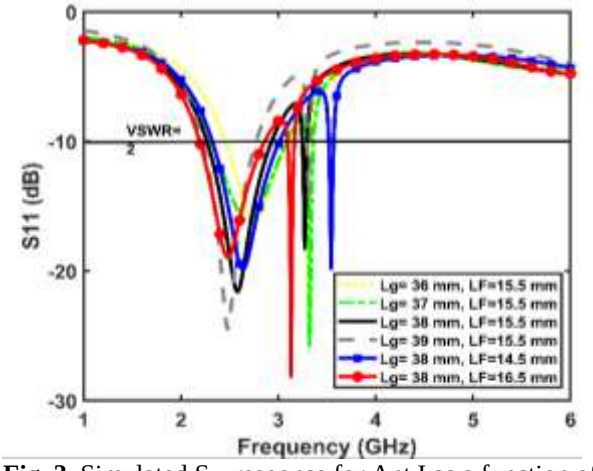

Fig. 3. Simulated S_{11} response for Ant.I as a function of parameters L_g and L_F.

Second, simulated S_{11} response of the Ant. II is presented in Fig. 4 which is obtained by adding a stub to the ground plane. It is clear that by varying the length of the stub (L_s) and the gap between the stub and feed line (g_s), the impedance bandwidths of the antenna is improved significantly. The frequency bandwidth ($S_{11}\leq$ -10 dB) is covered for the optimal values of L_s= 12 mm and g_s= 1 mm, which are obtained from the parametric analysis, in the range of 2.4 GHz to 3.8 GHz.

The return loss coefficient of Ant. II is shown in Fig. 5. By adding a meandered strip line as extra current path to the inverted F patch and tuning its key parameters of it, double frequency bands are established at the 1.5GHz to 2.3 GHz and 3.1GHz to 3.8 GHz. It is clear that by changing W_1 and L_{s2}, the upper band is less sensitive to the mentioned parameters compared to the lower band.

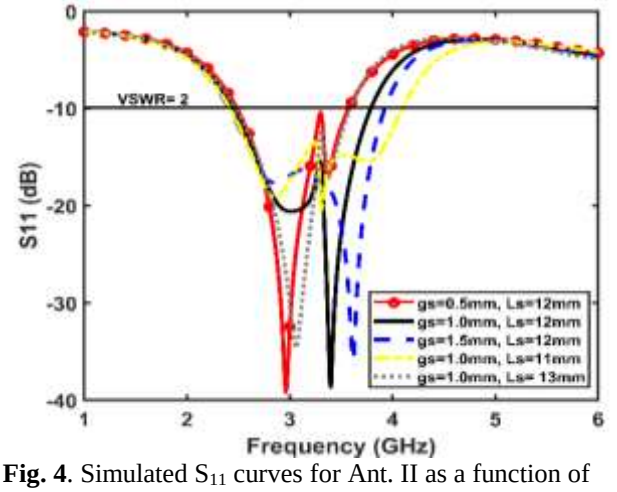

Fig. 4. Simulated S_{11} curves for Ant. II as a function of L_s and g_s.

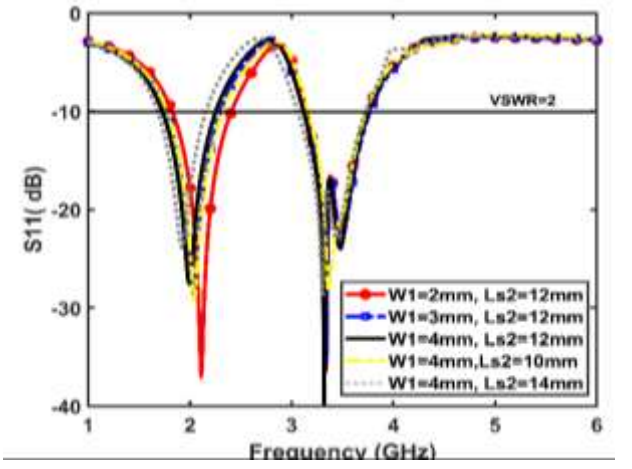

Fig. 5. Simulated S_{11} curves for Ant. II as a function of W_1 and L_{s2}.

On the other hand, the third resonance mode of Ant. IV at the WLAN and LTE 2500 band is produced by adding a strip line to the Ant. III while the preceding two frequency bands are fixed. Extracted return loss coefficient of the Antenna is depicted as a function of L_{s6} and L_{s3} in Fig. 6 while keeping other parameters unchanged at optimum values of the aforementioned antenna evolution. It is clear that, the impedance bandwidth of antenna ($S_{11}<$ -10dB) operates at triple frequency bands including 1.5 GHz to 2.3 GHz, 2.39 GHz to 2.65 GHz, and 3.2 GHz to 3.8 GHz.

Finally, the last frequency band is obtained by inserting the SCSRR metamaterial unit-cell next to the feed line and under the modified inverted patch on the substrate, which ultimately caused the antenna to act as a quad-band functionality. The first specification of the SCSRR unit-cell was designed to operate at 5.5 GHz. The structure is then added to Ant. IV along with a stub on the ground for better impedance matching (Ant. V). Fig. 7 demonstrates the S11 response of Ant.V as a function of the position of the structure on the substrate (Lgm) and the length of the stub (Lsm), while keeping other parameters fixed at their optimal values. It is obvious that the antenna resonates in the frequency range of 5.15 GHz to 5.75 GHz in addition to other frequency bands.

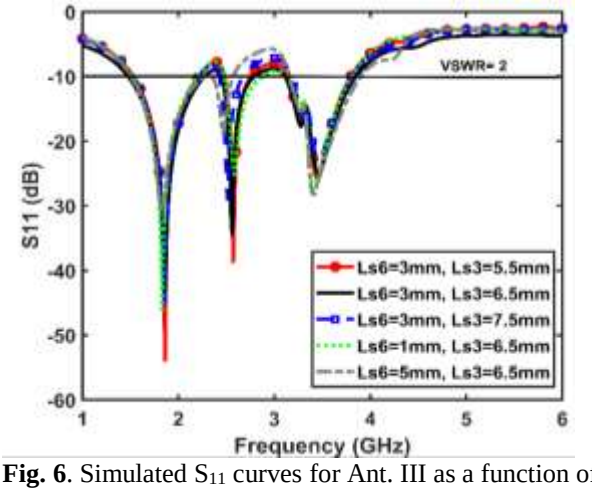

Fig. 6. Simulated S_{11} curves for Ant. III as a function of L_{s6} and L_{s3}.

For better evaluation of antenna performance, return loss coefficient curves of antenna phases with optimal values are illustrated in Fig. 8. The final proposed antenna (Ant. V) covers the frequency bands of LTE 1800, LTE 1900, UMTS, LTE 2300, LTE 2500, WLAN specified by IEEE 802.11a/b/g/n/ac and WiMAX.

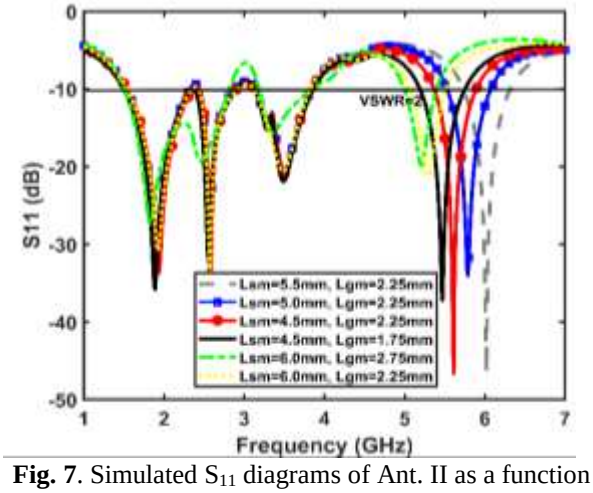

Fig. 7. Simulated S_{11} diagrams of Ant. II as a function of L_{gm} and L_{sm}.

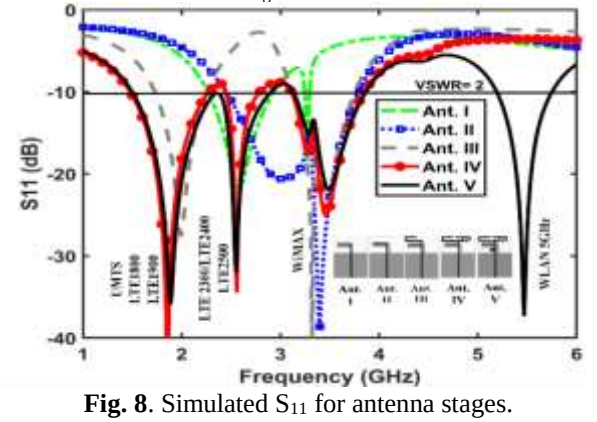

Fig. 8. Simulated S_{11} for antenna stages.

The extracted radiation patterns of the final antenna (Ant. V) at the center frequency of each band are shown in Fig. 9 for phi equal to 0 (E plane) and 90 (H plane) degrees. The radiation pattern at 1.89 GHz, 2.55 GHz is nearly bi-directional in the E plane, whereas it is nearly omnidirectional in H-plane. Also, the radiation pattern at 3.5 GHz is approximately heart-shaped in the E plane and omnidirectional in H-plane. Similarly, the E-plane and H-plane radiation pattern at 5.47 GHz almost has a semi-directional pattern.

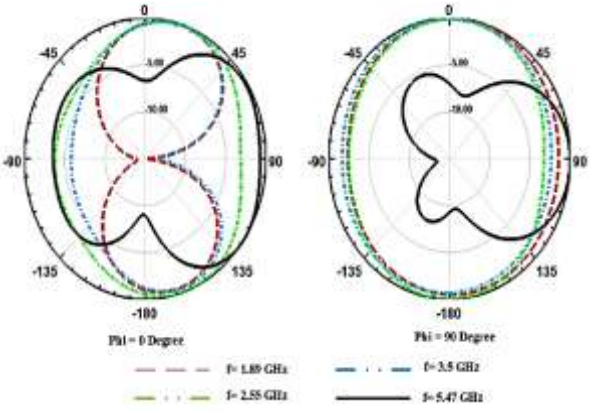

Fig. 9. Extracted radiation patterns of the final antenna (Ant. V) at the defined frequency.

3. MODIFIED PIFA MIMO DESIGN

In this section, the proposed monopole antenna has been used for 2×2 MIMO configuration which are previously studied. Fig. 10 shows the final MIMO antenna with the main parameters along with its development steps. The main challenge in MIMO antenna design is to overcome the mutual coupling between its radiation elements, especially in the lower bands because of the restriction of the antenna dimensions. The antennas occupied 50×70×0.8 mm^3 of substrate size while realized on FR-4 material with the dielectric constant of 4.4.

In this work, the mutual coupling is reduced using a combination of concepts including the placement of the radiation elements relative to each other, the defective ground structure (DGS), and electromagnetic band gap (EBG) structures. To determine the EBG characteristics and verify the band-gap, 1×3 array of structures is placed between the two 50Ω open-ended microstrip-line (Fig. 11). One of the microstrip lines is employed to stimulate the surface wave, and other acts as the indicator of the electromagnetic field intensity [2]. Because of the EBG structures embedding, the magnitude of S21 significantly decreased at three ranges of 1.7–2.3GHz, 2.4-2.72GHz and 3.3–3.8 GHz. The reason for the size variation for the third ring is the Constructive interaction among rings and the excitation of the higher mode in the middle third band resonance. Return loss (S_{11}) and isolation coefficient (S_{21}) of MIMO antenna evolution

have been presented and compared in Fig. 12 and Fig. 13, respectively. It is clear that the proposed isolation structure achieves minimum mutual coupling below -20 dB at each frequency band while the MIMO antenna specifications, remain almost constant compared to a single antenna.

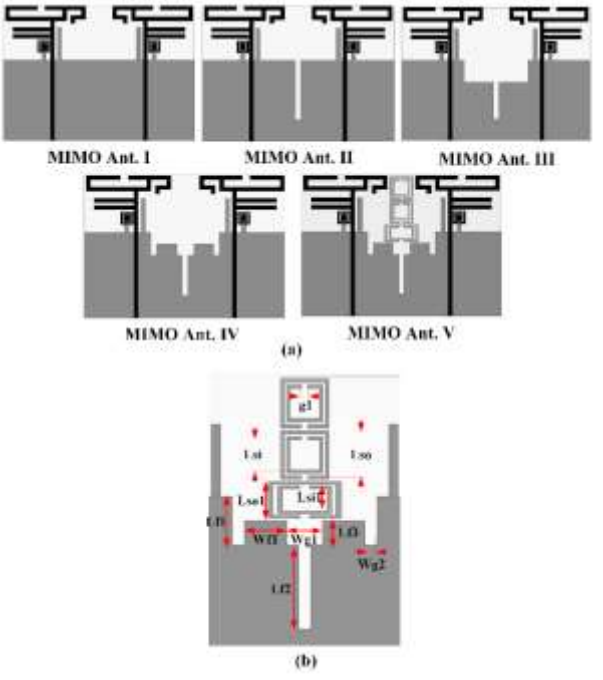

Fig. 10. (a) Final MIMO antenna with the main parameters along with its development steps (b) dimensions.

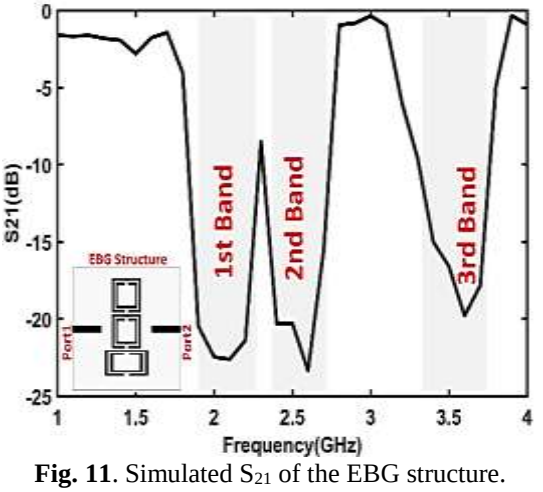

Fig. 11. Simulated S_{21} of the EBG structure.

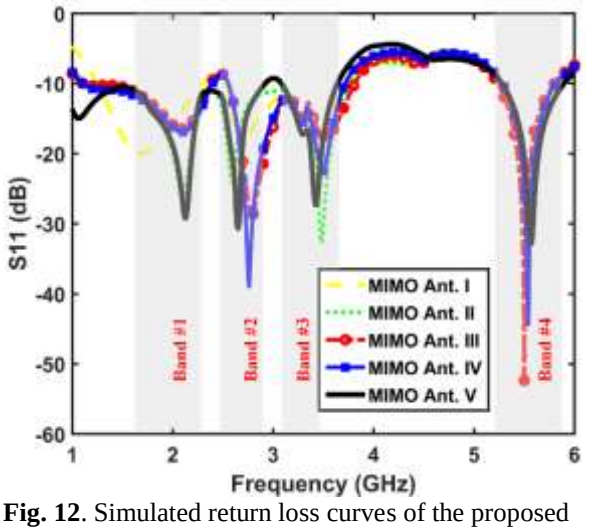

Fig. 12. Simulated return loss curves of the proposed MIMO antennas.

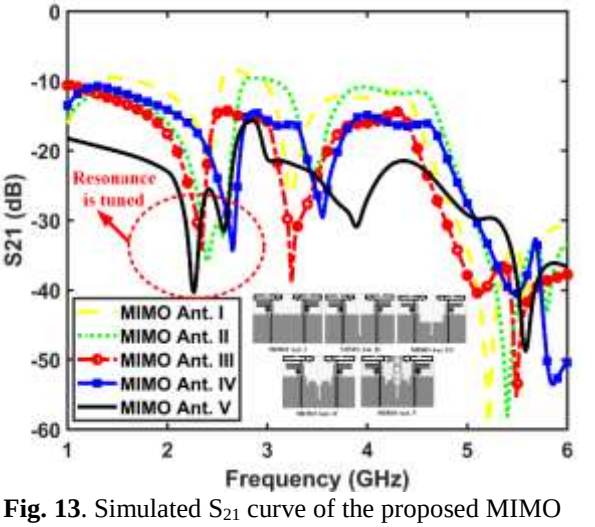

Fig. 13. Simulated S_{21} curve of the proposed MIMO antennas.

The extracted correlation coefficient of the MIMO multi-band antenna is depicted in Fig. 14. The correlation coefficient lies within the desired range, with a value of CC <0.3 for the MIMO multi-band antenna [21]. Fig. 15 illustrates the current distribution of the final suggested antenna at 1.89GHz, 2.55GHz, 3.5GHz & 5.47GHz. The effect of each part of the final structure on the formation of the mentioned resonances is shown in Fig. 15 according to the surface current distribution. Fig. 16 illustrates the radiation pattern of the ultimate MIMO Antenna at mentioned frequencies. Due to the acceptable performance of the filtering structure in reducing mutual coupling in the desired frequency bands, the single-element, and MIMO configuration have a good correlation in radiation patterns.

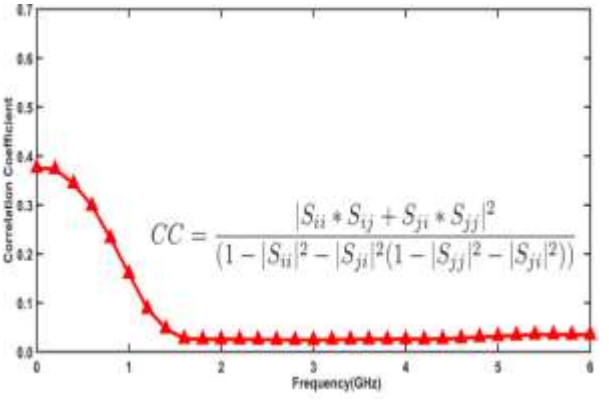

Fig. 14. Correlation coefficient of the proposed MIMO Antenna.

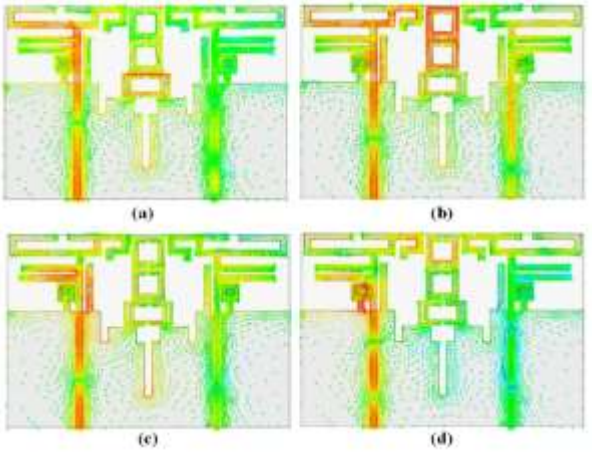

Fig. 15. Current distribution of the final proposed antenna (a) 1.9 GHz (b) 2.4 GHz (c) 3.5 GHz (d) 5.5 GHz.

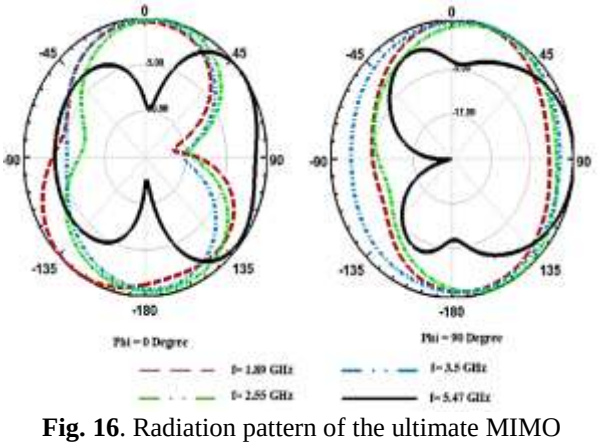

Fig. 16. Radiation pattern of the ultimate MIMO Antenna

4. CONSTRUCTION AND MEASUREMENT RESULTS

In this section, MIMO antenna is constructed by optimal values and the results of scattering parameters, gain, axial ratio, and radiation patterns are presented. For this purpose, first, the antenna is fabricated as shown in Fig. 17, then the antenna scattering parameters (S_{11} & S_{21}) are measured using the vector network analyzer KeySight PNA-X N5242A. The scattering parameters curves of MIMO Antenna (return loss and mutual coupling) have been measured and compared to the simulated results as presented in Fig. 17. It is apparent that the bandwidth specification necessities of LTE (1800, 2100, 2300, and 2500), WiMAX and WLAN bands are fully achieved while there is mostly good agreement between the measurement and simulation results. However, small deviations between the measured and simulated return losses are associated with fabrication tolerance, dispersion property of the non-ideal substrate, and soldering of SMA to the antenna.

Fig. 18 shows the Axial Ratio of the realized MIMO antenna. As can be seen, in the frequency bands of 1.8-2.15GHz, 2.45-2.6 GHz, 3.4-3.55 GHz, and 5.2-5.7 GHz, circular polarization property is achieved. Fig. 19 illustrates the simulated and measured peak gain of the ultimate fabricated Antenna. The peak gain average values, for all of the operational bands, are approximately at 6 dBi.

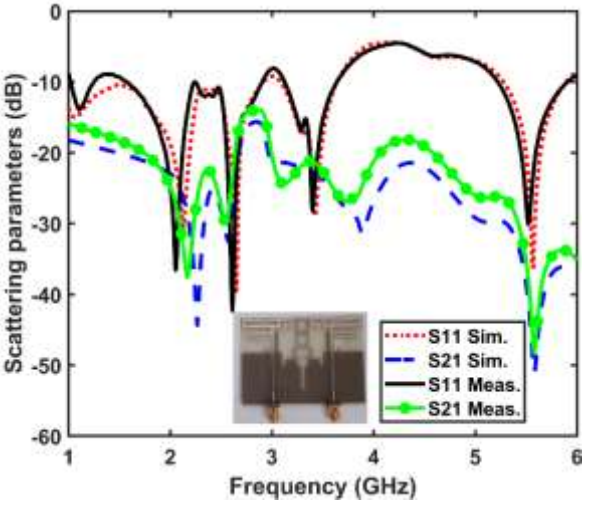

Fig. 17. Scattering parameters of the fabricated antenna.

Finally, the extracted right-handed circular polarized (RHCP) and the left-handed circular polarized (LHCP) radiation patterns for phi=0& 90 degrees of the antenna at the frequencies of 1.89, 2.55, 3.5 and 5.47 GHz are shown in Fig. 20. It is clearly seen that the radiation patterns are almost Omni-directional patterns at H-plane and the E-planes are monopole-like. Table II shows that the proposed 2×2 MIMO antenna performance is compared to the other reported similar antenna systems in the literature.

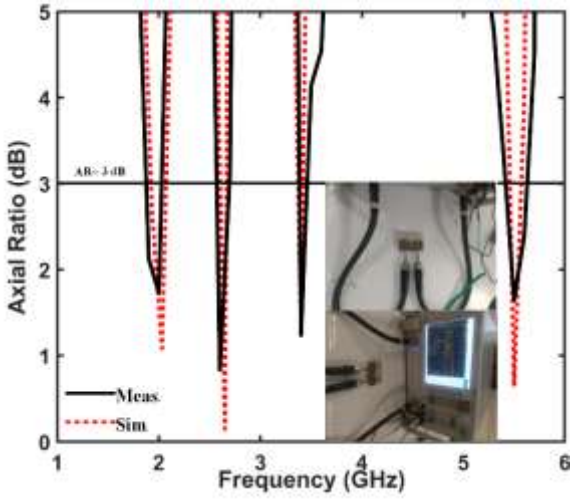

Fig. 18. Axial Ratio of realized antenna scattering parameters of the fabricated antenna.

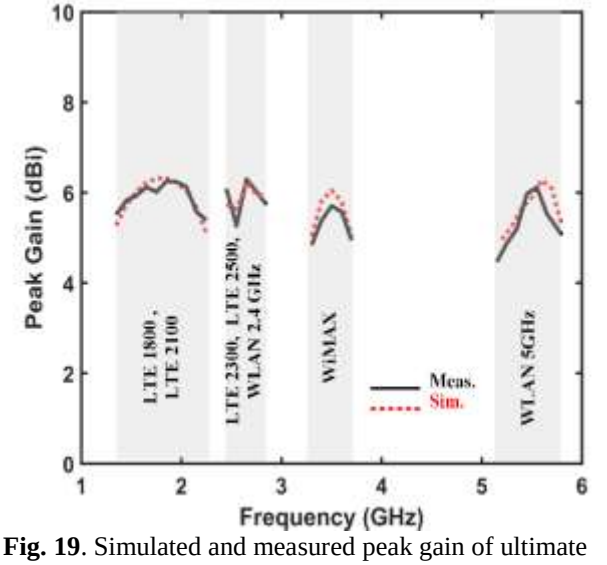

Fig. 19. Simulated and measured peak gain of ultimate fabricated Antenna.

5. CONCLUSION

A MIMO Quad-band modified antenna is introduced for mobile applications. Multiband functionality is achieved using a combination of methods of current path deviation, such as SCSRR and EBG structure at the final platform. The multi-band antenna Covers LTE 1800 (1.71-1.88 GHz), LTE 1900 (1.85-1.99 GHz), UMTS (1.92-2.17 GHz), LTE 2300 (2.305-2.40 GHz), LTE 2500 (2.50-2.69 GHz), WLAN (2.40-2.484 GHz- 5.15-5.75 GHz) specified by IEEE 802.11a/b/g/n/ac and WiMAX (3.3–3.6 GHz). PIFA MIMO is used as 2×2 array as a radiation element. The whole dimensions of a single antenna are 50×35×0.8 mm^3 and the MIMO antenna is 50×70×0.8 mm^3 while both are realized on FR4-epoxy substrate. To decrease destructive mutual coupling at MIMO geometry, defected ground structure (DGS) along with parasitic double split ring resonator are used. The MIMO antenna characteristics are validated by the realization of the prototype and measuring its performance in terms of axial ratio, reflection loss, and gain. The results prohibit well correlation between the experimental and simulation results. Overall, the proposed system is a fantastic applicant for mobile and wireless communications.

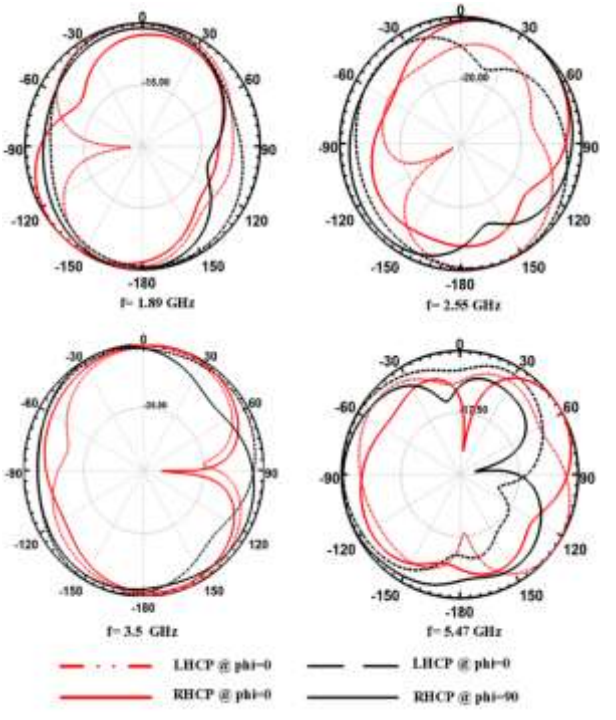

Fig. 20. Extracted RHCP & LHCP radiation patterns for phi=0& 90 degrees of the antenna at the frequencies of 1.89, 2.55, 3.5 and 5.47 GHz

6. ACKNOWLEDGMENT

The authors would like to appreciate Microwave & Antenna Research Center of Islamic Azad University Urmia Branch for measuring the device

Table II. Comparison between this work and related previous works.

Reference	MIMO	Operating frequency bands (G Hz)	Max S21 (dB) at bands	Size (mm^3)	Mobile communication standards							
					3G and LTE					WiMAX	WLAN	
					1800	1900	UMTS	2300	2500		2.4 GHZ	5 GHZ
[3]	2×2	2.25-3.32 3.32-3.74	-22.69 -18.43	71×42 ×0.8	×	×	×	✓	✓	✓	✓	×
[11]	2×2	2.57-2.64 5.72-5.82	-20.48 -20.4	40×75 ×1.6	×	×	×	×	✓	×	×	✓
[12]	2×2	1.71-2.2 2.4-2.48 2.5-2.69	-21.5 -22.5 -25.6	110× 65× 0.8	✓	✓	✓	×	✓	×	✓	×
This Work	2×2	1.71-2.17 2.305-2.4 2.4-2.484 2.5-2.69 3.3-3.6 5.15-5.75	-31.42 -22.48 -24.41 -26.7 -21.81 -48.32	50×35 ×0.8	✓	✓	✓	✓	✓	✓	✓	✓

REFERENCES

[1] R. Khajeh Mohammad Lou, M. Naser-Moghadasi, and R. A. Sadeghzadeh, "Compact Multi-Band Circularly Polarized CPW Fed Antenna Based on Metamaterial Resonator," Wireless Personal Communications, vol. 94, no. 4, pp. 2853-2863, 2017

[2] T. Sedghi, T. Aribi, and A. Kalami, "WiMAX and C bands semi-fractal circularly polarized antenna with satellite bands filtering properties," International Journal of Microwave and Wireless Technologies, vol. 10, no. 8, pp. 978-983, 2018

[3] L. Tchoketch-Kebir and B. Tlili, "Dual band MIMO microstrip monopole antenna with enhanced bandwidth for LTE applications," in 2014 Loughborough Antennas and Propagation Conference (LAPC), 10-11 Nov. 2014, pp. 249-253

[4] M. Naser-Moghadasi, R. A. Sadeghzadeh, R. K. MohammadLou, M. Jalali, and B. S. Virdee, "Miniature Planer Monopole Antenna with Dual-Band Rejection Characteristics for UWB Applications," Microwave and Optical Technology Letters, vol. 55, no. 9, pp. 1977-1981, 2013

[5] M. Rezvani and Y. Zehforoosh, "Design of Multi-band Microstrip Antenna for Wireless Communications and ITU Applications," National Academy Science Letters, vol. 40, no. 5, pp. 331-334, 2017

[6] H. Wen, Y. Qi, Z. Weng, F. Li, and J. Fan, "A Multiband Dual-Polarized Omnidirectional Antenna for 2G/3G/LTE Applications," IEEE Antennas and Wireless Propagation Letters, vol. 17, no. 2, pp. 180-183, 2018

[7] F. A. Asadallah, J. Costantine, and Y. Tawk, "A Multiband Compact Reconfigurable PIFA Based on Nested Slots," IEEE Antennas and Wireless Propagation Letters, vol. 17, no. 2, pp. 331-334, 2018

[8] P. Beigi, J. Nourinia, Y. Zehforoosh, "Compact CPW-fed spiral-patch monopole antenna with tuneable frequency for multiband applications," Journal of Instrumentation, vol. 13, no. 4, pp. 1-8, 2018

[9] J. Dong, X. Yu, and L. Deng, "A Decoupled Multiband Dual-Antenna System for WWAN/LTE Smartphone Applications," IEEE Antennas and Wireless Propagation Letters, vol. 16, pp. 1528-1532, 2017

[10] R. Khajeh Mohammad Lou, M. Naser-Moghadasi, and R. A. Sadeghzadeh, "Broadband Planar Aperture-Coupled Antenna Array for WLAN and ITS Beam-Steering Applications," Radio Science, vol. 53, no. 2, pp. 200-209, 2018

[11] S. Y. P. Cahyanto and E. Y. D. Utami, "Planar Multiband MIMO Antenna for LTE and WLAN Applications," in 2018 International Seminar on Intelligent Technology and Its Applications (ISITIA),

30-31 Aug. 2018, pp. 5-8

[12] S. Shoaib, I. Shoaib, N. Shoaib, X. Chen, and C. G. Parini, "MIMO Antennas for Mobile Handsets," IEEE Antennas and Wireless Propagation Letters, vol. 14, pp. 799-802, 2015

[13] X. Zhou, X. Quan, and R. Li, "A Dual-Broadband MIMO Antenna System for GSM/UMTS/LTE and WLAN Handsets," IEEE Antennas and Wireless Propagation Letters, vol. 11, pp. 551-554, 2012

[14] F. Ahmed, R. Li, and Y. Feng, "Development of a compact planar multiband MIMO antenna for 4G/LTE/WLAN mobile phone standards," in 2013 Proceedings of the International Symposium on Antennas & Propagation, 23-25 Oct. 2013 2013, vol. 01, pp. 539-542.

[15] S. Wang and Z. Du, "A Dual-Antenna System for LTE/WWAN/WLAN/WiMAX Smartphone Applications," IEEE Antennas and Wireless Propagation Letters, vol. 14, pp. 1443-1446, 2015

[16] R. Anitha, P. V. Vinesh, K. C. Prakash, P. Mohanan, and K. Vasudevan, "A Compact Quad Element Slotted Ground Wideband Antenna for MIMO Applications," IEEE Transactions on Antennas and Propagation, vol. 64, no. 10, pp. 4550-4553, 2016

[17] J. Lu, H. Chin, and Z. Lin, "Planar monopole antenna with triple-band operation for LTE/WLAN MIMO system," in 2017 IEEE International Conference on Computational Electromagnetics (ICCEM), 8-10 March 2017, pp. 318-319.

[18] T. Aribi, M. Naser-Moghadasi, and R. A. Sadeghzadeh, "Circularly polarized beam-steering antenna array with enhanced characteristics using UCEBG structure," International Journal of Microwave and Wireless Technologies, vol. 8, no. 6, pp. 955-962, 2016

[19] M. I. Ahmed, A. Sebak, E. A. Abdallah, and H. Elhennawy, "Mutual coupling reduction using defected ground structure (DGS) for array applications," in 2012 15 International Symposium on Antenna Technology and Applied Electromagnetics, 25-28 June 2012, pp. 1-5

[20] C. Zhao, X. Li, C. Sun, and H. Huang, "Reduction of mutual coupling between patch antennas using defected ground structure in L- and S-bands," Microwave and Optical Technology Letters, vol. 61, no. 12, pp. 2730-2738, 2019

[21] K. Wei, J. Li, L. Wang, Z. Xing, and R. Xu, "Mutual Coupling Reduction by Novel Fractal Defected Ground Structure Bandgap Filter," IEEE Transactions on Antennas and Propagation, vol. 64, no. 10, pp. 4328-4335, 2016

[22] M. Al-Hasan, I. B. Mabrouk, E. R. F. Almajali, M. Nedil, and T. A. Denidni, "Hybrid Isolator for Mutual-Coupling Reduction in Millimeter-Wave MIMO Antenna Systems," IEEE Access, vol. 7, pp. 58466-58474, 2019

[23] G. Exposito-Dominguez, J. Fernandez-Gonzalez, P. Padilla, and M. Sierra-Castaner, "Mutual Coupling Reduction Using EBG in Steering Antennas," IEEE Antennas and Wireless Propagation Letters, vol. 11, pp. 1265-1268, 2012.